Resolution Enhancement with High Transmission Attenuating Phase Shift Masks

Robert J. Socha, Will E. Conley, Xuelong Shi, and Mircea V. Dusa
National Semiconductor Corp., 2900 Semiconductor Dr., Santa Clara CA 95051-8090
e-mail: Robert.Socha@nsc.com

John S. Petersen
Petersen Advanced Lithography, P.O. Box 162712, Austin, TX 78716

Fung Chen, Kurt Wampler, Tom Laidig, Roger Caldwell
MicroUnity Systems Engineering Inc., 475 Potrero Ave., Sunnyvale, CA 94086-4118

1.   Abstract

Experiments to print 140nm lines and 140nm contact holes were optimized through simulation on an 18% transmitting phase shift mask for KrF lithography. A transmittance of 18% is to improve aerial image log slope through focus for the lines and contacts. The 140nm lines for all three pitches have a maximum depth of focus of at least 0.90μm. The exposure latitude of the 140nm lines is over 7.5% for all pitches to maintain 0.6μm depth of focus. Experiments show that the 140nm and 160nm contact holes resolve without side lobe printing through focus and through exposure. Reticle SEMs verify that a ternary contact hole mask is capable of manufacture. By adding both opaque and clear sub-resolution assist features, the experiments show contacts as small as 140nm resolve with 0.50μm focus latitude with 10% exposure latitude through pitch. Cross sectional SEMs verify that 140nm contact holes are open through pitch. Simulations to quantify the MEF show that the MEF for attenuating PSM decreases as the transmittance of the attenuating material increases. The MEF for a 30% transmitting attenuating material is 1.90 for a 150nm feature and the MEF for an alternating PSM is 1.42 for the same 150nm feature. Trends in aerial image CD variation due to aberrations were simulated for focal plane deviation, x coma, astigmatism, and spherical aberrations. The simulations of alternating PSM imaged with σ of 0.35 suggest that alternating PSM have the least CD variation due to focal plane deviation, astigmatism, and coma for dense pitches. The CD variation due to coma is comparable to 33% transmittance attenuating PSM for isolated lines. Furthermore alternating PSM is more susceptible to CD placement error due to coma compared to attenuating PSM. The 33% transmittance attenuating PSM has the least CD variation due to spherical aberration in comparison to BIM and alternating PSM.

2.   Introduction

In order to push a 248nm wavelength exposure tool to print sub wavelength features, the tool must be capable of printing both lines and contacts. In this paper, the feasibility of printing both sub wavelength lines and contact holes is discussed by using a high transmission attenuated phase shift mask with KrF lithography. The use of attenuated phase shift masks to improve the depth of focus is well known from the literature [1][2]. Two high transmission attenuating phase shift masks were designed through simulation to print 140nm lines and 140nm contact holes. Several techniques in designing these masks have been considered. All of these techniques use a ternary attenuating phase shift mask where ternary implies three tones; the quartz blank, the attenuated phase shift background material, and chrome (opaque) assist features. The addition of the chrome assist features improves image log slope, which improves the image resolution through focus. In addition to the improved resolution, the chrome on the contact hole attenuating phase shift mask suppresses side lobe printing.

The technique used in designing a ternary attenuating phase shift mask for lines is based on extending the use of assist features used on binary masks to attenuating phase shift masks [3,4]. The use of assist features on a binary reticle has been show to improve the depth of focus for isolated lines. The improved process latitude of isolated lines is overlapped with dense lines through fine biasing to improve

the overlapping process window. In this paper, the improved depth of focus and resolution of the lines are shown through experiments in Section 4.

The use of a ternary attenuating phase shift reticle for contact hole printing is based on extending the use of serifs and chrome assist features on an i-line contact hole mask developed by Chen [5] to DUV, the use of Bessel contact phase structures by Schellenburg [6,7], RIM attenuated PSM structures described by Ma [8] and high transmission phase shift masks by Iwasaki [9]. The later two types of RIM structures by Schellenburg, Ma and Iwasaki where found to give the best resolution capable of printing 140nm contacts as predicted by simulation. In these RIM structures, the assist features are very large, and only relatively isolated contacts can be printed. The technique by Chen, however, allows an increase in contact hole density with a reduction in the process window in order to print 140nm features with 0.5μm pitch. This technique was used to design a high transmission ternary attenuating phase shift reticle through simulation to print 200nm, 170nm, and 140nm contact holes using a 248nm wavelength exposure tool [10]. A reticle designed through these simulations was fabricated and printed with experimental results described in this paper in Section 6 and reference 11.

In gate line printing, the use of alternating phase shift mask for improved depth of focus and for improved CD control has been demonstrated [12,13]. The extent that the transmission of an attenuating phase shift mask impacts the critical dimension (CD) control, however, has yet to be demonstrated. The CD control is a function of many variables. The type of reticle enhancement effects both the mask error factor (MEF) and the CD variation due to the aberrations. The impact of aberrations and the MEF can be determined by understanding the interaction of the diffraction orders with the lens and illumination. In this paper, the CD variation due to the MEF and to the aberrations is predicted through simulations in Sections 7 and 8, respectively.

3.   Design of the Line Resolution Mask

The use of an attenuating phase shift mask for printing lines reduces the zero order light and increases the first order light in comparison to binary masks. The combination of zero order reduction and first order improvement increases the contrast through focus. This increased contrast is directly related to the improved resolution through focus. The improvement in contrast with the use of attenuating PSM is demonstrated through simulation in Figure 1. In Figure 1 the aerial image of a 150nm semi-isolated line at 0.0μm focus and 0.50μm focus is simulated for a binary mask, a binary mask with scattering bar OPC, 5% transmittance attenuating PSM with chrome scattering bar OPC and 18% transmittance attenuating PSM with chrome scattering bar OPC. The simulations are done with NA of 0.55 and weak quad off axis illumination. The aerial images at 0.0μm and 0.5μm focus have increasing image log slope as the transmittance of the phase shift mask increases. This improved log slope results in increased resolution and depth of focus.

The use of opaque scattering bars on a ternary high transmission phase shift mask further improves the depth of focus (DOF). In Figure 2, the resist image of a 120nm line with 840nm pitch is simulated for a 6% and 18% transmission attenuating phase shift mask without OPC and with scattering bar OPC (SB OPC). In comparing the simulated CD results without OPC and with SB OPC, the scattering bar OPC reduces the curvature of the Bossung plot through focus. This reduction in curvature leads to better depth of focus with SB OPC. Furthermore, as shown in Figure 1, the log slope of the aerial image increases as transmittance increases. This increase in log slope leads to improved depth of focus. This improved depth of focus is shown in Figure 2. In Figure 2, the curvature of the Bossung plot is less with 18% transmittance in comparison to 6% transmittance PSM.

4.   Experimental Results from the Line Resolution Mask

The simulation results discussed in Section 3 are confirmed through experiments in this section. An attenuating PSM with 18% transmittance was exposed with a KrF tool on UV5 and UV70 on top of AR2 over bare poly silicon. The UV5 had a thickness of 550nm, and the UV70 had a thickness of 420nm. The two resists were processed with standard soft bake and post exposure bake time and temperatures. Both resists were soft baked at 130°C for 60 seconds with a post exposure bake at 130°C for 90 seconds. Four illumination conditions were tested all with a NA of 0.63. These illumination conditions were conventional σ=0.8, conventional σ=0.65, conventional σ=0.30 and annular 0.5/0.8. The 140nm lines were measured for pitches of 440nm, 780nm and 1340nm. The structures consisted of five line patterns and the center line was always measured. On the reticle, the 440nm pitch features received no OPC treatment while the pitch of 760nm and 1340nm both received SB OPC. The SB OPC was optimized to improve the depth of focus

for each pitch while also maximizing the process window overlap of the three pitches. The reticle design is shown in Figure 3 for each of the pitches. In all the data taken the scattering bars never printed.

Top down SEM results of the 140nm lines for the three pitches of 440nm, 760nm, and 1340nm with UV70 are shown in Figure 4, Figure 5, and Figure 6, respectively. The top down SEMs were exposed with a NA of 0.63 and a σ of 0.8. The focus latitude is displayed vertically and the exposure latitude horizontally. In the figures, the maximum depth of focus, the maximum exposure latitude, the exposure latitude at 0.6μm depth of focus, and the depth of focus at 10% exposure latitude is reported for all three pitches. The 140nm lines for all three pitches have a maximum depth of focus of at least 0.90μm. In addition to the focus latitude, the exposure latitude to maintain 0.6μm depth of focus is over 7.5% for all pitches. By reducing the DOF requirement, it was possible to increase the exposure latitude. It is possible to increase this exposure latitude by tuning the OPC for a particular NA and σ, and by tuning the photoresist to sample the aerial image at an optimal intensity threshold. For all the pitches the best energy for the individual process windows is between 12.3mJ/cm^2 and 12.9mJ/cm^2. An exposure between these energies allows for 4.52% overlapping exposure latitude for all three pitches with 0.5μm depth of focus requirement when the exposure is centered at 12.66mJ/cm^2 and focus of -0.33μm. The overlapping exposure latitude was improved in subsequent experiments by redesigning the reticle for high NA and high σ and by tuning the photoresist for the aerial image contrast.

The results with UV5 and UV70 for σ of 0.65 and 0.8 with a NA of 0.63 are summarized in Table 1. In Table 1, the maximum depth of focus, the maximum exposure latitude, the exposure latitude at 0.6μm depth of focus, and the depth of focus at 10% exposure latitude is reported for all three pitches. Comparing results of the two different resists, the illumination and resist with the largest overlapping process window was UV70 with conventional illumination of σ 0.8. For all three pitches, this process also had the best overlapping exposure latitude of 4.52% for a 0.5μm DOF requirement. This process was also the only process to having a common window for 10% exposure latitude with although it only had 0.15μm DOF. Although, the illumination of σ 0.35 was exposed, it had less than 0.60μm max DOF and are not reported in Table 1. Each individual pitch with the annular illumination did have the best exposure latitudes at 0.6μm DOF; however, there was no common process window for all three pitches. The overlapping exposure latitude with annular illumination was improved in further experiments by redesigning the reticle for a particular annular setting.

In addition to 140nm lines, the 120nm lines resolve through pitch. The proximity effects through pitch for these lines are plotted in Figure 7, Figure 8, Figure 9, and Figure 10. Results without OPC and for an exposure of 13.6mJ/cm^2 and 14.2mJ/cm^2 are shown in Figure 7 and Figure 9, respectively. Results with OPC and for an exposure of 13.6mJ/cm^2 and 14.2mJ/cm^2 are shown in Figure 8 and Figure 10, respectively. In comparing Figure 7 and Figure 8 for an exposure of 13.6mJ/cm^2, the SB OPC reduces the spread through focus of the 0.70μm spaces and 2μm spaces. This indicates that the SB OPC improves the depth of focus of the isolated lines as the resist samples the aerial image near the isofocal point. The OPC with an exposure of 13.6mJ/cm^2 in Figure 8 shows a spread of 30nm through focus for the isolated lines (space of 2.0μm). This spread through focus can be reduced to less than 15nm by slightly overexposing to 14.2mJ/cm^2 as shown in Figure 10. Slightly overexposing the lines without OPC in Figure 9, however, does not reduce the CD spread of isolated lines through focus since the lines do not resolve. The results of the denser pitches with and without OPC, however, show about 15nm spread due to effects. This large CD spread is due to a lack of fine biasing on the reticle. The reticle was written on an 80nm grid at 4X magnification. This writing grid only allows a minimum bias of 20nm.

5.   Design of the Contact Hole Mask

From the theory of the optimal contact hole design in references 10 and 11, the Bessel contact hole reticle was designed to have the greatest resolution possible through focus and through pitch. In this design, the possible transmissions and phases of the reticle must approximate the Bessel electric field. On a ternary mask, there are only three discrete steps to the transmission and phase. The first step is quartz glass, which has a transmittance of 100% and a phase of 0°. This clear quartz models the main lobe. The second step is attenuating phase shift material with transmittance to be chosen and a phase of 180°. The third step is chrome material, which has 0% transmittance. Squaring the first minimum of the Bessel electric field establishes the transmittance and phase of the attenuating material. In Figure 11, the electric field as a function of position is plotted for three cases at 0.0μm focus. These cases are: NA of 0.63 and σ of 0.35; NA of 0.60 and σ of 0.35; and NA of 0.63 and σ of 0.50. In comparing the magnitude of the

electric field in the peaks and valleys in Figure 11, σ causes the magnitude of the first minima to change; however, NA has little effect on magnitude of the first minima. Furthermore, since lower σ has better resolution and better depth of focus, this reticle was designed for σ of 0.35. The electric field magnitude of the first minima is approximately 0.38 for σ of 0.35. Therefore, the best choice of the transmittance of the attenuating phase shift material is approximately 15% (the square of 0.38). The previous argument is correct to get the best resolution at 0.0μm focus. However, the resolution must be maintained through focus. In order to maintain the resolution through focus, simulations were done to find the optimal transmittance through focus. Results of the simulations are shown in Figure 12. Since the peak intensity is related to the resolution, the peak intensity is plotted in Figure 12 as a function of focus for variable transmittance. For a transmittance between 16% to 20% the peak intensity is flattest through focus. This implies that the size of the printed contact hole will not oscillate through focus for a 16% to 20% transmittance range. Consequently, a transmittance of 18% was used for this reticle. Since the side lobes other than the first side lobe have a small electric field magnitude (0.2 or 4% transmittance), the secondary side lobes are modeled with the chrome. This chrome essentially removes the zero order light, which improves the resolution and depth of focus. The chrome also has another beneficial effect of preventing side lobe printing.

In addition to approximating the transmission and phase of the electric field, the shape of the electric field and the locations of maxima and minima must be designed by making the electric field discrete. Since the pupil is circular, the electric field is radially symmetric; consequently, the optimal shape of the contact hole is circular as well. Since the hole is made on a discrete square grid for some reticle writing tools, the circular contact hole was approximated with both octagon holes and square holes. Finally, the transitions from quartz to attenuating material to chrome must be defined. This was done through simulation as described in reference 10. This is described briefly here. Attenuating phase shifted material as shown in Figure 13 surrounds a square isolated contact. This attenuating material represents the first side lobe and the chrome surrounding the hole represent the other side lobes. The size of the contact hole and the width of the attenuating phase shifted material are optimized by simulation. The width of the attenuating material is optimizing by maintaining constant peak intensity through focus. This is shown in Figure 14 in which the peak intensity is plotted as a function of focus for variable frame scattering bar distance (fSB). The definition of the frame scattering bar distance is shown in Figure 13 and is simply the width of the attenuating phase shift material. Figure 14 shows that the optimal fSB is 0.18μm for an isolated contact when exposing with a NA of 0.63 and a σ of 0.35.

Based on the previous arguments and the simulations of reference 10, the reticle layout was designed to meet the SIA roadmap contact hole values of 140, 170, and 200nm. The contact holes received OPC treatment of bias only and OPC treatment of bias with serifs. Scanning electron microscope (SEM) images were taken of the reticle. These SEM images are shown in Figure 15 for examples of typical Bessel contacts for various pitches.

6. Experimental Results from the Contact Hole Mask

The reticle described in Section 5 was printed on a wafer with a stack of material containing an anti reflective coating. An experimental DUV positive tone photoresist was used. Wafers with a NA of 0.60 and 0.63 were exposed with a σ of 0.35 on a KrF exposure tool. Top down SEM measurements were done with a VeraSEM from Applied Materials. Bossung plots and process windows were generated with ProData by Finle Technologies.

In the experiment, the 170nm contact holes with a 520nm pitch were slightly under exposed to achieve 160nm holes. Top down SEMs of the contact holes at the edge of the array are shown in Figure 16 for best exposure through focus and in Figure 17 for best focus through exposure. From Figure 16 of best exposure through focus, the holes from 0.0μm to +0.6μm are opening. Comparing the SEMs through focus and through exposure, there is no evidence of side lobe printing. On the reticle, the edge and corner of the array was corrected with optical proximity correction. The contact holes on the edge and in the corner show no evidence of proximity through focus and through exposure. This indicates that it is possible to correct the contact holes on a typical product reticle in which the holes are neither fully dense nor fully isolated in both horizontal and vertical directions. After importing the data into ProData, a process window with 0.51μm depth of focus at 10% exposure latitude is expected. Although, the process window for the 680nm pitch is not shown, the process windows of the 520nm pitch and the 680nm pitch do not overlap.

The lack of overlapping windows is due to the fact that the resist model is slightly incorrect. By slightly changing the resist process, it is expected to get overlapping process windows.

In addition to the 170nm contacts, the 140nm contacts through pitch were also resolved. Cross section SEMs of the 140nm contact holes through pitch are shown in Figure 18 for best focus and best exposure. The SEMs indicate that the 140nm holes are resolving through pitch. The SEMs also show that the resist profile is nearly vertical with some standing waves. The standing waves indicate that the anti reflection coating needs to be optimized.

The exposure and dose latitude of the 140nm contacts is shown in Figure 19 and Figure 20 for a pitch of 500nm and 1400nm, respectively. The 500nm pitch has 0.6μm depth of focus at 10% exposure latitude and the process window is centered at 30mJ/cm^2 and +0.20μm focus. The isolated pitch of 1400nm has 0.51μm depth of focus at 8.4% exposure latitude, and its window is centered at 38.4mJ/cm^2 at +0.22μm focus. As in the case of the 160nm contacts, the exposure windows of the 140nm contacts are slightly off in dose. Once again by slightly changing the resist process, it is expected to get overlapping process windows.

7.   Mask Error Factor (MEF) Simulations

The MEF was simulated using TEMPEST[14] in order accurately model the mask topography. The aerial image line width was then extracted at an aerial image intensity threshold. The MEF for the 0.18μm, 0.15μm, and 0.13μm isolated mask lines is plotted in Figure 21 for three mask transmittances of 0% (BIM), 5% attenuating PSM, and 30% attenuating PSM. The aerial images were simulated at a focus of 0μm, a NA of 0.63, and a σ of 0.75. The image line width was sampled at a 0.3 intensity threshold for the binary mask (BIM) and at a 0.25 threshold for all the phase shift masks. The MEF in Figure 21 is the slope of the line when the mask CD is plotted versus aerial image CD. For each mask line width, the MEF is reported next to each mask CD for the three mask types. The MEF for BIM increases as the mask CD decreases. The MEF for BIM of a 0.18μm line width is 2.0 while the MEF for a 0.13μm BIM line width is 3.1. The 3.1 MEF implies that 10nm CD errors on the mask at 1X result in 31nm CD errors on the wafer. These MEF results are only based on aerial image simulations and do no model the photoresist effect. The simulations of the attenuating PSM show that MEF decreases as the transmittance of the attenuating material increases. The MEF of the 0.15μm lines is 2.3 with 5% transmittance and 1.9 with 30% transmittance. The MEF for attenuating PSM for 0.13μm features reduces to 2.8 with 5% and 2.0 with 30%. The reduction in the MEF as transmittance increases implies improved wafer CD uniformity due to reticle CD errors. The reduced MEF and the improved process latitudes with high transmission attenuating PSM indicates that high transmission attenuating masks may be a suitable technology for gate level in addition to metal and via levels.

In order to become a suitable gate level technology, the MEF of high transmission attenuating PSM must be comparable to the MEF of alternating PSM, which has demonstrated exceptional CD uniformity. The MEF of 30% transmission attenuating PSM is compared through aerial image simulation to the MEF of alternating PSM and the MEF of binary mask (BIM) in Figure 22. In Figure 22, the MEF of the attenuating PSM is near 2.0 for all feature dimensions of 0.18μm, 0.15μm and 0.13μm. The MEF of the BIM as discussed in the previous paragraph increases as the feature dimension decreases. The MEF of the alternating PSM, however, decreases as the feature size decreases. The MEF of a 0.15μm feature is 1.4 while the MEF of a 0.13μm feature decreases further to 1.0. This implies that a 10nm mask error at 1X of an alternating PSM for the 0.13μm technology node results in a 10nm error on the wafer as predicted by aerial image simulation. Although the MEF of the alternating PSM is less than the MEF of attenuating PSM as predicted by simulation, the photoresist which samples the aerial image impacts the wafer MEF. Further experiments in the fab need to be done to quantify the photoresist effect on the MEF for both alternating PSM and high transmission PSM.

8.   Aberration Simulations on CD Uniformity

In addition to the MEF, aberrations impact the CD uniformity. In order to quantify the impact of aberrations on CD uniformity, simulations were performed with Prolith by Finle Technologies. The effect of aberrations on aerial image line width were simulated for 140nm lines with three pitches of 440nm, 760nm, and 1340nm. Six types of masks were simulated and these include BIM, 5% Att. PSM, 18% Att. PSM, 30% Att. PSM, Alt. PSM imaged with low σ (σ=0.35), and Alt. PSM imaged with high σ (σ=0.75). In all the simulations a NA of 0.63 was used with a σ of 0.75 for the BIM and attenuating PSM

simulations. Four types of aberration were simulated and include focus, astigmatism, x coma, and spherical. The aerial image line width was measured at the 0.3 intensity threshold for BIM and 0.25 threshold for all the Att. PSM and Alt. PSM simulations. When the curvature of the aerial image line width is the flattest as a function of the aberration, the CD uniformity is least susceptible to the aberration. In addition to measuring the line width variation, the image position shift is reported for coma. Although other radial unsymmetrical aberrations will produce position shift, only x coma had an effect since the lines were orientated along the y axis.

The first aberration simulated is focus. Focus was simulated to develop a baseline to compare the simulation results of the other aberrations. The aerial image line width is plotted as a function of focus in μm as shown in Figure 23. The curvature of this plotted line indicates the impact of the focus on the CD uniformity. A line that is flat through focus indicates that CD uniformity is least susceptible to focal plane deviation. The BIM for a relatively isolated pitch of 1340nm has aerial image line width deviation from 120nm to 80nm for 40nm total CD deviation over a 0.3μm focus range. As the pitch decreases for the BIM, the curvature increases for BIM and implies that the focal plane deviation causes more CD variation for dense pitches. The 760nm pitch for BIM has 58nm total CD deviation while the 440nm pitch has 76nm deviation. The attenuating PSM has less curvature than the BIM, which indicates that attenuating PSM has better DOF than BIM as shown in the experimental results of Section 4. The pitch of 1340nm has approximately 37nm total CD deviation for the 5% Att. PSM, 25nm total deviation for the 18% Att. PSM, and 20nm total deviation for the 33% Att. PSM. This indicates that as the transmittance increases the impact of focal plane deviation on CD uniformity decreases. As the pitch decreases, the high transmittance attenuating PSM material continues to have the least amount of CD deviation due to focus. The CD variation for all the attenuating PSM materials slightly increases as pitch decreases. For example, the 33% transmittance material has 24nm CD variation for a pitch of 760nm and 30nm CD variation for a pitch of 440nm over 0.3μm focal range. The increased CD variation is due to the fact that as the pitch decreases the outer portion of the lens are being sampled. The outer portion of the lens have the greatest optical path difference (OPD) through focus and consequently cause more CD variation. The alternating PSM was imaged with two partial coherence factors to determine the impact of σ on CD variation. The σ of 0.75 for the alternating PSM has the greatest amount of curvature through pitch. This curvature causes CD variation of 38nm, 58nm, and 80nm for 1340nm pitch, 760nm pitch and 440nm pitch, respectively. In comparing the alternating PSM with high σ to the BIM, alternating PSM with high σ has the greatest CD variation due to focal plane deviation. However, as σ decreases, the CD variation due to focal plane deviation decreases when imaging an alternating PSM. Through pitch the CD variation due to focal plane deviation is less than 10nm when imaging an alternating PSM with a σ of 0.35. This reduction in CD variation through focus is due to sampling the aerial image CD at an intensity near the isofocal point. In conclusion, the alternating PSM when imaged with a low σ has the least CD variation through.

The effect of astigmatism on CD variation for a 140nm line was also simulated for the same three pitches. The aerial image line width is plotted as a function of astigmatism in number of wavelengths (λ) in Figure 24. As in the case of focus, the curvature of the plotted line indicates the impact of astigmatism on CD uniformity with a flat line having better CD uniformity. As in the case of focus, the BIM has large CD variation due to astigmatism, and the CD variation increases as pitch decreases. For the BIM, the total CD variation for the 1340nm pitch is 51nm for 0.2λ of astigmatism, 58nm CD variation for the 760nm pitch, and 76nm CD variation for the 440nm pitch. Again the CD variation is increasing as pitch decreases because the light samples more of the outer portion of the lens. For the attenuating PSM, the curvature of the line is less than the curvature of the line for BIM. This indicates that an attenuating PSM is least susceptible to the impact of astigmatism on the CD variation in comparison to the BIM. As the transmittance of the attenuating PSM increases, the impact of astigmatism on CD variation decreases. For example, the isolated pitch of 1340nm with 5% transmittance suffers from 40nm total CD variation over 0.2λ of astigmatism while the 33% transmittance suffers from 30nm total CD variation over the same 0.2λ of astigmatism. In addition to the impact of transmittance on CD variation, the pitch has an impact on CD variation as well. The 33% transmittance PSM has 30nm CD variation over 0.2λ astigmatism for a pitch of 1340nm which increases to 37nm CD variation for a pitch of 440nm. This indicates that as pitch decreases the impact of astigmatism of CD variation increases. Lastly the effect of astigmatism on CD variation for an alternating PSM is discussed for a σ of 0.75 and 0.35. The alternating PSM when imaged with σ of 0.75 has the greatest amount of curvature through waves of astigmatism. From Figure 24, the line width is 0nm for all pitches when 0.2λ of astigmatism is present in the lens. This indicates that the alternating PSM

when imaged with high σ has the greatest CD variation due to astigmatism. However, as σ decreases, the CD variation due to astigmatism decreases when imaging an alternating PSM. When imaging an alternating PSM with low σ, the CD variation due to astigmatism drops to fewer than 10nm for all three pitches. As with the impact of focal plane deviation, alternating PSM imaged with low σ is least susceptible to astigmatism.

The effect of x coma on CD variation and on image CD position for a 140nm line was also simulated for the same three pitches. The aerial image line width and the CD position is plotted as a function of coma in number of wavelengths (λ) in Figure 25 and Figure 26, respectively. As the coma aberration increases, the CD variation increases for the BIM. In Figure 25, the total CD deviation for 0.2λ of coma is 40nm, 42nm and 55nm for the pitch of 1340nm, 760nm and 440nm, respectively. This indicates that as pitch decreases the CD variation increases for the BIM. In addition to the CD variation, the x coma causes CD position shift in lines oriented along the y axis. From Figure 26, 0.1λ of coma causes 20nm of CD position shift for the 1340nm pitch. Furthermore, as the coma increases and the pitch decreases, the CD position shift increases. For attenuating PSM, the CD variation decreases as the transmittance increases. This is demonstrated in Figure 25 in which a 5% transmittance for a pitch of 1340nm has approximately 37nm CD loss for 0.2λ of coma and a 33% transmittance has 30nm CD loss. The improvement, however, in CD uniformity with an increased transmittance is exchanged for increased position error with an increase in transmittance. Again from Figure 26, 0.1λ of coma for a pitch of 1340nm causes 23nm of CD position shift for 5% transmittance in comparison to 30nm of CD shift for the 33% transmittance. Lastly the effect of coma on CD variation and on image position error is discussed for an alternating PSM when imaging with a σ of 0.75 and 0.35. The alternating PSM when imaged with σ of 0.75 has the greatest amount of curvature as a function of waves of coma. From Figure 25, 0.2λ of coma causes the CD to decrease by 38nm, by 59nm, and by 60nm for pitches of 1340nm, 760nm, and 440nm, respectively. In comparison to the BIM where the CD decreases by 40nm, 42nm and 55nm CD for the pitches of 1340nm, 760nm, and 440nm, coma has the greatest impact on CD variation on an alternating PSM when imaged with high σ. For the alternating PSM, the CD variation due to coma decreases, however, when imaging with a σ of 0.35 in comparison to the σ of 0.75. This is seen in Figure 25 for the σ of 0.35 in which 0.2λ of coma causes 29nm and 35nm total CD variation for the pitch of 1340nm and 760nm, respectively. This CD variation with alternating PSM is comparable to the CD variation with 33% transmittance attenuating PSM, which has 30nm, and 31nm total CD variation for the pitches of 1340nm and 760nm, respectively. Although the coma causes CD variation to increase for the more isolated alternating PSM features, the CD variation for the 440nm pitch caused by coma is less than 10nm for alternating PSM imaged with σ of 0.35. As in the case of the high transmittance attenuating PSM, the improvement in CD uniformity of the low σ alternating PSM over the high σ alternating PSM is exchanged for CD position error. At 0.1λ of coma, the alternating PSM imaged with a σ of 0.35 causes over 40nm of CD placement error in comparison to the 10nm of CD placement error of alternating PSM imaged with a σ of 0.75. In conclusion, coma causes comparable CD variation for high transmittance attenuating PSM and for alternating PSM, and coma causes less CD placement error with attenuating PSM than with alternating PSM.

The effect of spherical aberration on CD variation for a 140nm line was also simulated for the same three pitches. The aerial image line width is plotted as a function of spherical aberration in number of wavelengths (λ) in Figure 27. The BIM for the isolated pitch of 1340nm has 70nm of CD variation due to 0.2λ of spherical aberration. This CD variation increases to 78nm and 120nm as the pitch decreases to 760nm and 440nm, respectively. For the attenuating PSM, the curvature of the line is less than the curvature of the line for BIM. This indicates that an attenuating PSM as compared to BIM is less susceptible to the impact of spherical aberration on the CD variation. As the transmittance of the attenuating PSM increases, the impact of spherical aberration on CD variation decreases. For example, the isolated pitch of 1340nm with 5% transmittance suffers from 55nm total CD variation over 0.2λ of spherical aberration while the 33% transmittance suffers from 50nm total CD variation over the same 0.2λ of spherical aberration. In addition to the impact of transmittance on CD variation, the pitch has an impact on CD variation as well. The 33% transmittance PSM has 55nm CD variation over 0.2λ spherical aberration for a pitch of 1340nm which decreases to 48nm CD variation for a pitch of 440nm. This indicates that as pitch decreases the impact of spherical aberration on CD variation decreases for high transmission attenuating PSM. Lastly the effect of spherical aberration on CD variation for an alternating PSM is examined for a σ of 0.75 and 0.35. An alternating PSM when imaged with σ of 0.35 has the more

curvature through waves of spherical aberration in comparison to an alternating PSM when image with σ of 0.75. For an alternating PSM with a 1340nm pitch in Figure 27, 0.2λ of spherical aberration cause 115nm of CD variation when imaging with σ of 0.35 in comparison to 80nm of CD variation when imaging with σ of 0.75. Furthermore, as the pitch decreases on an alternating PSM, the CD variation increases for both σ conditions. Contrary to the other aberrations, spherical aberration causes more CD variation in an alternating PSM in comparison to BIM and attenuating PSM. In conclusion, the high 33% transmittance attenuating PSM suffers from the least amount of CD variation due to spherical aberration.

9. Conclusions

Experiments with an 18% transmittance phase shift mask prove that 140nm lines and 140nm contacts resolve with production worthy process margin on a KrF lithography tool. These experiments further indicate the value of simulation in optimizing the design of the ternary PSM line reticle and the design of the ternary PSM contact hole reticle. On the ternary PSM line reticle, the addition of chrome scattering bars lowers the isofocal point, which improves the depth of focus for isolated lines and improves the overlap between the isolated and dense features. On the ternary PSM contact hole reticle, the chrome eliminates side lobe printing and is an essential optical element in improving resolution.

The 140nm lines on the ternary PSM have a maximum depth of focus of at least 0.90μm through pitch. In addition to the focus latitude of the 140nm lines, the exposure latitude to maintain 0.6μm depth of focus is over 7.5% for all pitches. Initial experiments presented in this paper show poor overlapping process windows because the OPC and the resist were not tuned to a particular optical setting. In subsequent experiments, the overlapping exposure latitude was improved by redesigning the reticle for high NA and high σ and by tuning the photoresist to sample a particular aerial image contrast for the type of optical enhancement.

On the ternary PSM contact hole reticle, the resolution and the pitch density is also strongly influenced by NA and σ. Contrary to the lines, the NA also impacts the exposure latitude of the contact holes but has little impact on the depth of focus. This lack of impact on depth of focus is due to the Bessel contact hole design in which the width of the annulus in the pupil plane influences depth of focus. Since σ controls the width of the annulus, σ has the largest impact on depth of focus as indicated by theory, simulation, and experiment.

The optical proximity correction reduces the contact size variation and reduces the line width variation between isolated and dense features. The experiments, however, show some problems with the process window overlap through pitch for the 140nm lines and contacts. The lack of overlap is due to the interaction effects between elements of the complete lithography system. The elements of the complete lithography system include the reticle, the illumination and projection optics, and the resist. In order to push lithography into sub wavelength printing, the interaction between these parts of the total lithography system must be understood.

The results for printing lines and contacts holes with attenuating PSM show a strong need for high transmittance materials to improve resolution and depth of focus. High transmittance PSM materials are needed to extend KrF lithography to print sub wavelength contact hole layers and metal layers. Experiments still need to be done to determine the CD uniformity of high transmittance reticles for the gate layer. Simulations, however, show that the MEF decreases as the transmittance increases. Furthermore, simulations show that the impact of aberrations on CD variation with high transmittance attenuating PSM is competitive with alternating PSM. If the simulations accurately predict the CD variation, high transmittance attenuating PSM will be used on the 0.13μm gate layer generation.

10. References

1. B. Lin, "Phase-shifting and other challenges in optical mask technology," Proc. SPIE, Vol. 1496, pp. 54-79 (1990).
2. T. Terasawa et. al., "Image characteristics of multi-phase-shifting and halftone phase shifting masks," Jpn. J. Appl. Phy., Vol. 30.
3. J. F. Chen, T. Laidig, K. E. Wampler, R. Caldwell, Proc. SPIE Vol. 3051, p.790 - 803 (1997).
4. J. F. Chen, T. Laidig, K. E. Wampler, R. Caldwell, JVST B 15(6), Nov/Dec p. 2426 - 2433 (1997).
5. F. Chen, et. al., "Practical I-line OPC contact masks for sub 0.3 micron design rule applications," Proc. Of Olin Interface, p. 181 (1997).

6.   F. Schellenberg, et. al., "Optimization of real phase mask performance," Proc. of SPIE, Vol. 1604, p. 274 (1991).
7.   F. Schellenberg, et. al., "Real and Imaginary Phase-Shifting Masks," Proc. of SPIE, Vol. 1809, p. 237 (1992).
8.   Z. M. Ma, et. al., "Preventing sidelobe printing in applying attenuated phase shift reticles," Proc. of SPIE, Vol. 3334 (1998).
9.   H. Iwasaki, et. al., "High transmittance rim-type attenuated phase shift masks for sub-0.2µm hole patterns," Proc. of SPIE, Vol. 3412 (1998).
10.   R. Socha, et. al., "Design of 200nm, 170nm, 140nm DUV contact sweeper high transmission attenuating phase shift mask through simulation part 1," Proc. of SPIE, Vol. 3546 p. 617 (1998).
11.   R. Socha, et. al., "Design of 200nm, 170nm, 140nm DUV contact sweeper high transmission attenuating phase shift mask: experimental results part 2," Proc. of SPIE, Vol. 3679 (1999).
12.   H. Y. Liu, "The application of alternating phase-shifting masks to 140nm gate patterning: line width control improvements and design optimization," Proc. of SPIE, Vol. 3236, p. 328 (1998).
13.   G. Vandenberghe, et. al., "CD-control comparison for sub-0.18µm patterning using 248nm lithography and strong resolution enhancement techniques," Proc. of SPIE, Vol. 3679 (1999).
14.   A. Wong, "Tempest Users' Guide," Memorandum No. UCB/ERL M95/14, University of California, Berkeley, March 1995.
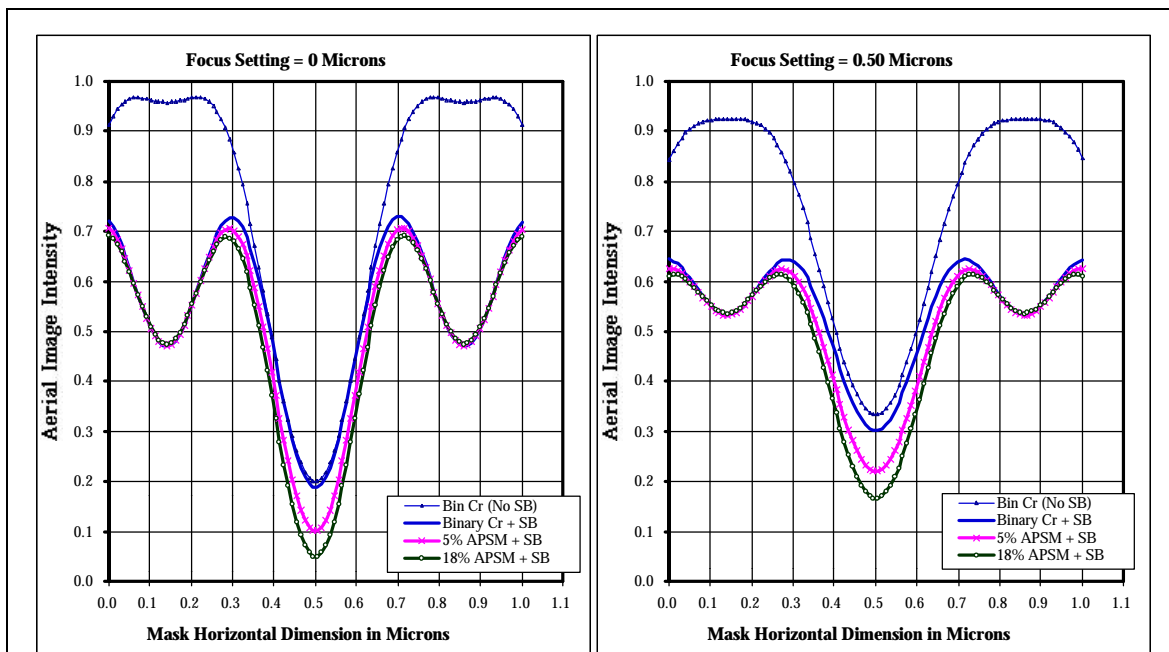
Figure 1. Effect of transmittance on aerial image contrast for 0.15µm features with 0.72µm pitch. The simulations were done with a NA of 0.55 and weak quad off axis illumination. The simulations show that as transmittance increases the contrast improves at 0.0µm focus and at 0.5µm focus. The improved contrast leads to improved focus latitude in the resist.
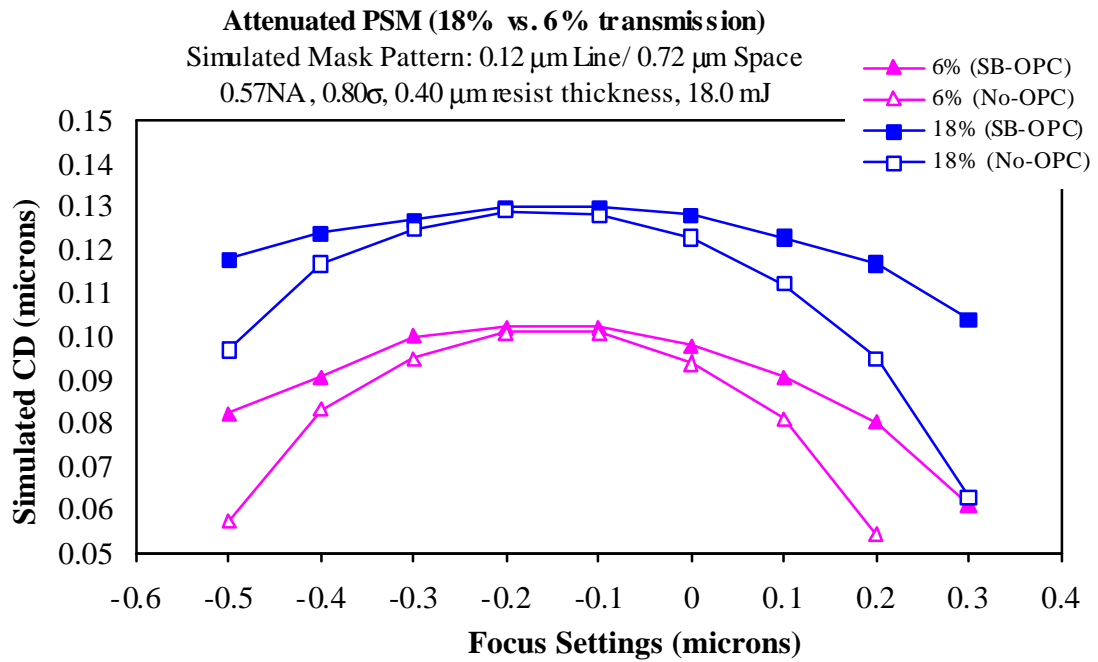
Figure 2. Simulations of the depth of focus improvement with opaque scattering bar OPC on an attenuating phase shift mask. The scattering bar OPC further increases the depth of focus in conjunction with increasing the transmittance of the PSM.

140nm line 300nm space
No OPC

SB Width 80nm

140nm line
620nm space SB
OPC

SB Width 60nm

Edge to Edge Separation 300nm

140nm line
1200nm
space SB
OPC

SB Width 80nm

Figure 3. Attenuating PSM mask design used in the experiments of Section 4. The gray features are the 140nm lines on the 18% transmittance Att. PSM. The black features are the sub-resolution chrome scattering bars.
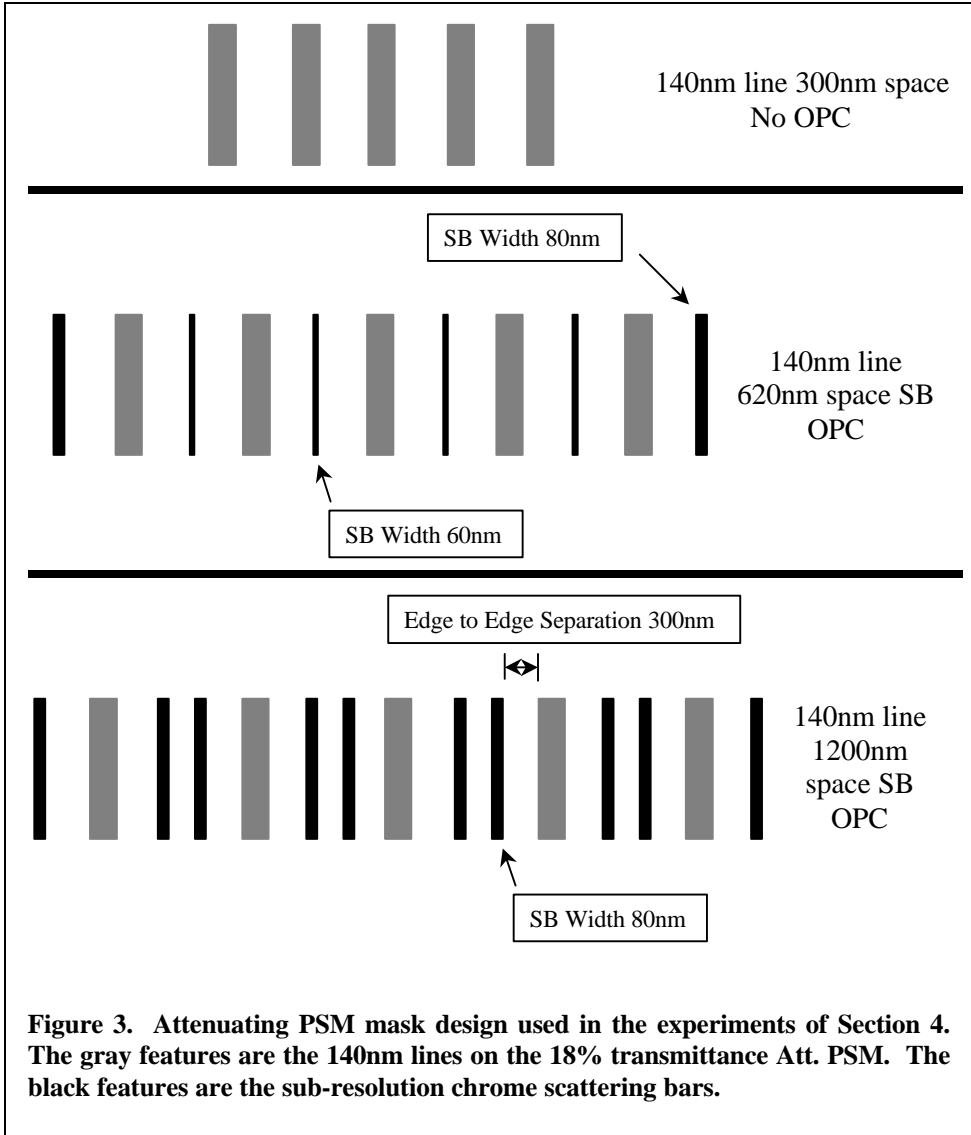
UV70 Top Down SEMs for 0.14μm line 1.2μm space

12.0mJ/cm²   12.5mJ/cm²   13.0mJ/cm²   13.5mJ/cm²

MaxDOF=0.90μm
MaxEL=20.27%

-0.75μm

DOF=0.6μm

Exp. Latitude=7.58%
Best Energy=12.87mJ/cm²
Best Focus=-0.24μm

-0.60μm

EL=10%

Focus Latitude=0.30μm
Best Energy=12.39mJ/cm²
Best Focus=-0.48μm

-0.45μm

-0.30μm

-0.15μm

0. 0μm

+0.15μm
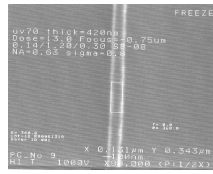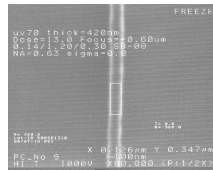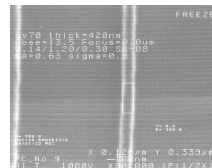
+0.30μm

Figure 4. Top down SEMs of 0.14μm lines in a pitch of 1.34μm. The exposure latitude is 7.6% for 0.6μm depth of focus requirement.

UV70 Top Down SEMs for 0.14μm line 0.62μm space

11.5mJ/cm²	12.0mJ/cm²	12.5mJ/cm²	13.0mJ/cm²

MaxDOF=1.13μm
MaxEL=12.96%

<u>DOF=0.6μm</u>
Exp. Latitude=8.67%
Best Energy=12.29mJ/cm²
Best Focus=-0.33μm

<u>EL=10%</u>
Focus Latitude=0.48μm
Best Energy=12.38mJ/cm²
Best Focus=-0.31μm

-0.75μm

-0.60μm

-0.45μm

-0.30μm

-0.15μm

0. 0μm

+0.15μm
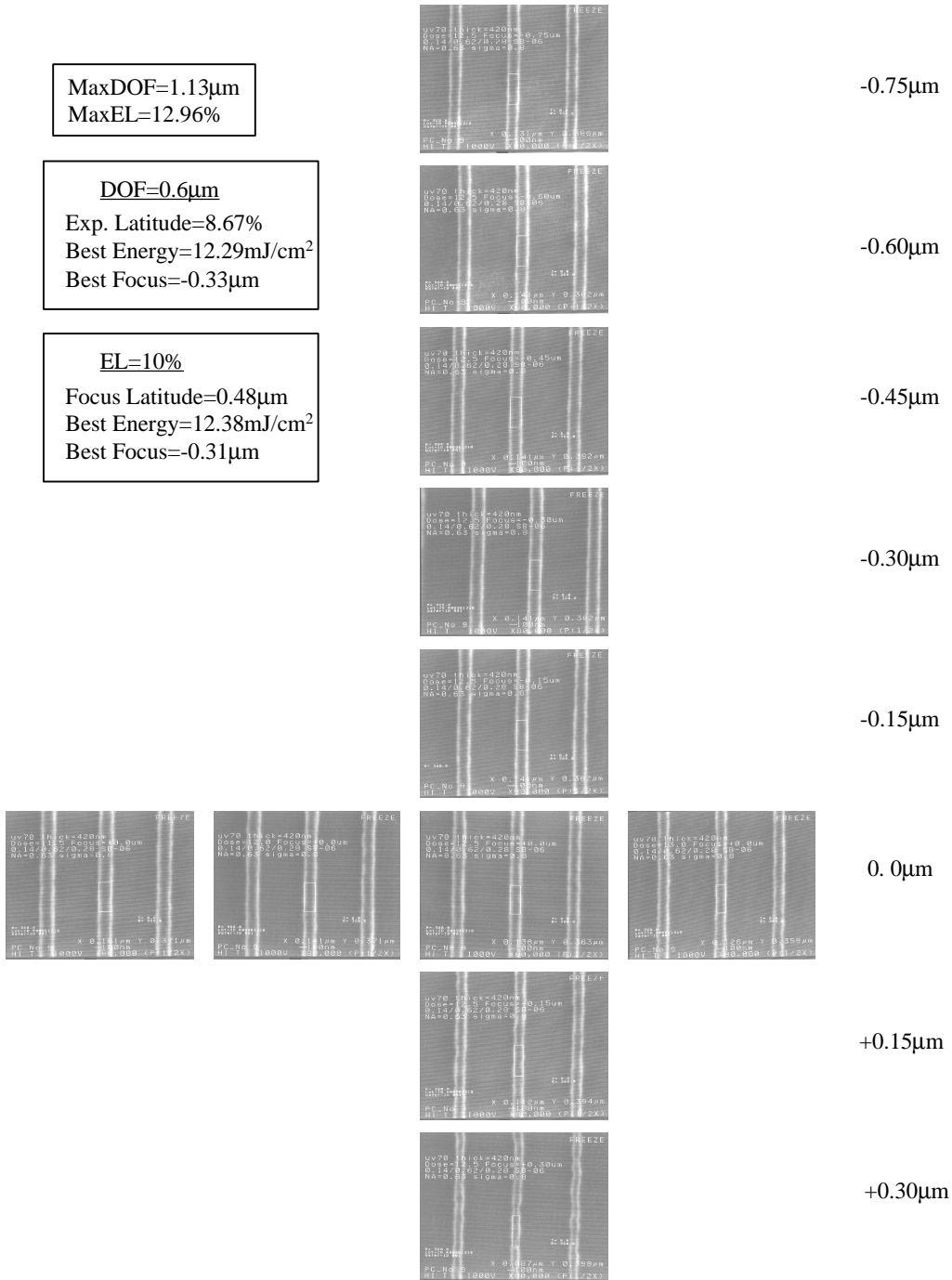
+0.30μm

Figure 5. Top down SEMs of 0.14μm lines in a pitch of 0.76μm. The exposure latitude is 8.7% for 0.6μm depth of focus requirement.

UV70 Top Down SEMs for 0.14μm line 0.30μm space

12.5mJ/cm^2 13.0mJ/cm^2 13.5mJ/cm^2 14.0mJ/cm^2
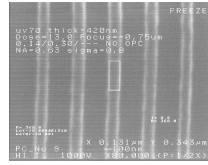
MaxDOF=1.35μm
MaxEL=15.55%

-0.75μm
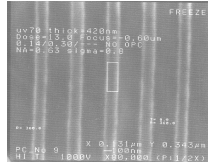
DOF=0.6μm
Exp. Latitude=8.98%
Best Energy=12.66mJ/cm^2
Best Focus=-0.33μm

-0.60μm
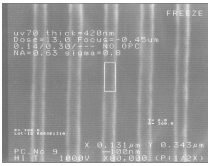
EL=10%
Focus Latitude=0.45μm
Best Energy=12.69mJ/cm^2
Best Focus=-0.35μm

-0.45μm
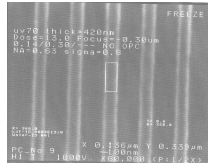
-0.30μm
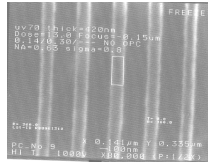
-0.15μm
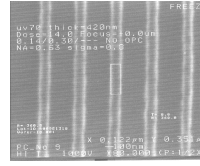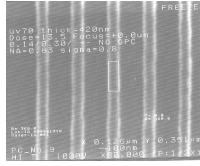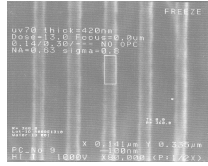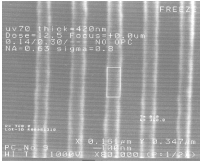
0. 0μm
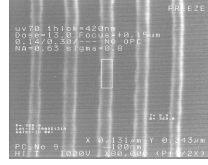
+0.15μm

+0.30μm

Figure 6. Top down SEMs of 0.14μm lines in a pitch of 0.44μm. The exposure latitude is 9.0% for 0.6μm depth of focus requirement.

Max DOF and Max Exposure latitude

Illumination	Space Width (μm)	Resist	Max DOF (μm)	Max Exp. Lat. %
sigma=0.8	0.30	UV70	1.35	15.55
		UV5	1.28	19.46
	0.62	UV70	1.13	12.96
		UV5	0.98	19.09
	1.20	UV70	0.90	20.27
		UV5	0.83	16.33
sigma=0.65	0.30	UV70	1.13	13.56
		UV5	1.05	11.56
	0.62	UV70	0.98	13.37
		UV5	0.90	13.75
	1.20	UV70	0.98	15.76
		UV5	0.90	13.35

DOF for 10% Exposure latitude

Illumination	Space Width (μm)	Resist	DOF (um)	Best Energy (mJ)	Best Focus (μm)
sigma=0.8	0.30	UV70	0.45	12.67	-0.35
		UV5	0.46	11.24	-0.14
	0.62	UV70	0.48	12.38	-0.31
		UV5	0.43	11.12	-0.14
	1.20	UV70	0.30	12.39	-0.48
		UV5	0.36	11.82	-0.08
sigma=0.65	0.30	UV70	0.53	12.30	-0.31
		UV5	0.32	11.26	-0.21
	0.62	UV70	0.39	12.75	-0.35
		UV5	0.18	11.81	-0.10
	1.20	UV70	0.47	13.11	-0.22
		UV5	0.36	11.76	-0.08

Exposure latitude for 0.6μm DOF

Illumination	Space Width (μm)	Resist	Exp. Lat. %	Best Energy (mJ)	Best Focus (μm)
sigma=0.8	0.30	UV70	8.98	12.66	-0.33
		UV5	9.08	11.19	-0.12
	0.62	UV70	8.67	12.29	-0.33
		UV5	5.51	10.86	-0.15
	1.20	UV70	7.58	12.87	-0.24
		UV5	5.52	11.55	-0.09
sigma=0.65	0.30	UV70	8.75	12.32	-0.30
		UV5	7.11	11.09	-0.18
	0.62	UV70	6.11	12.49	-0.36
		UV5	3.03	11.40	-0.12
	1.20	UV70	7.84	12.96	-0.24
		UV5	5.15	11.47	-0.09

Table 1. Exposure and focus latitudes with UV5 and UV70 for 0.14μm lines using a NA of 0.63 and a σ of 0.65 and 0.8.
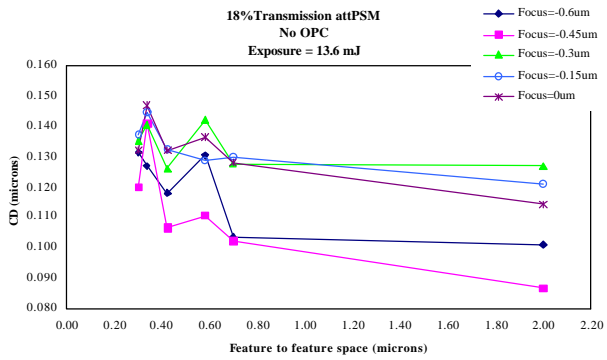
Figure 7. Proximity effects through pitch for120nm lines without OPC and 13.6mJ/cm^2.
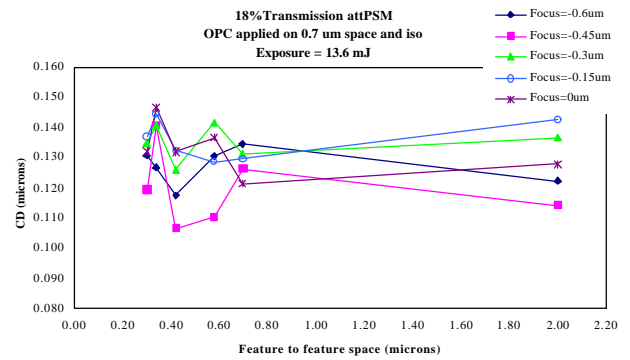
Figure 8. Proximity effects through pitch for120nm lines with OPC and 13.6mJ/cm^2.
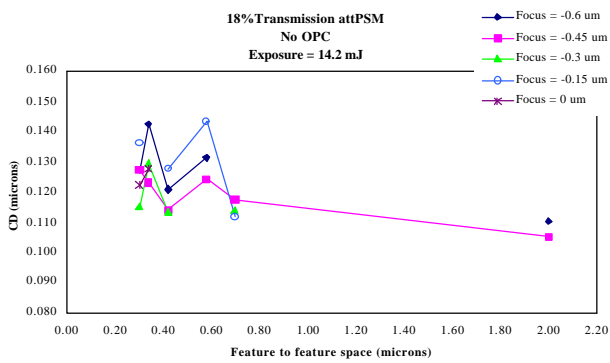
Figure 9. Proximity effects through pitch for120nm lines without OPC and 14.2mJ/cm^2.
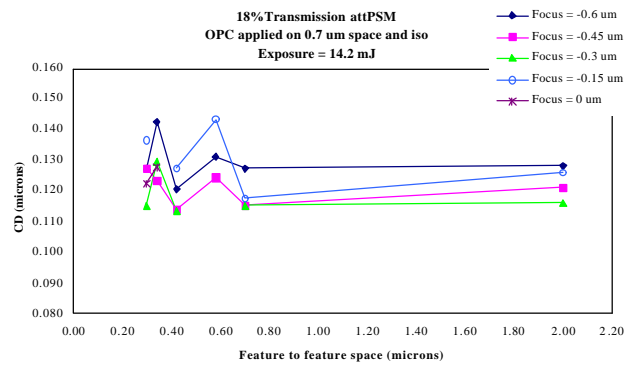
Figure 10. Proximity effects through pitch for120nm lines with OPC and 14.2mJ/cm^2.
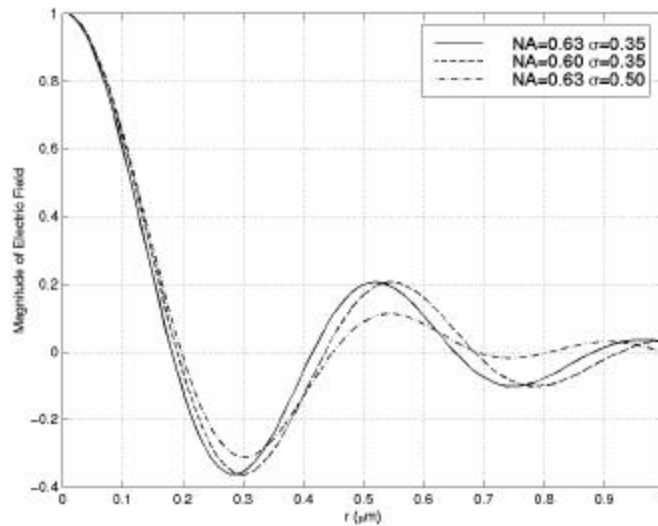
Figure 11. Effect of NA and σ on the electric field at 0.0µm focus. Note that as NA increases and σ decreases the resolution improves. The electric field amplitude made discrete in order to represent a Bessel contact on the mask.
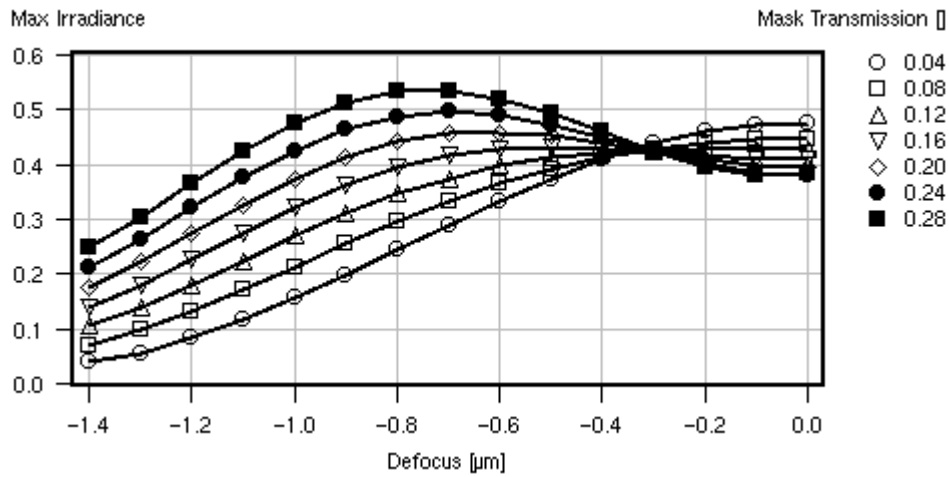
Figure 12. Effect of mask transmission (transmittance) on max irradiance (peak intensity) through focus. There are fewer oscillations for a transmittance between 16% to 20%. This transmittance range is optimal because the contact hole size will not oscillate through focus.
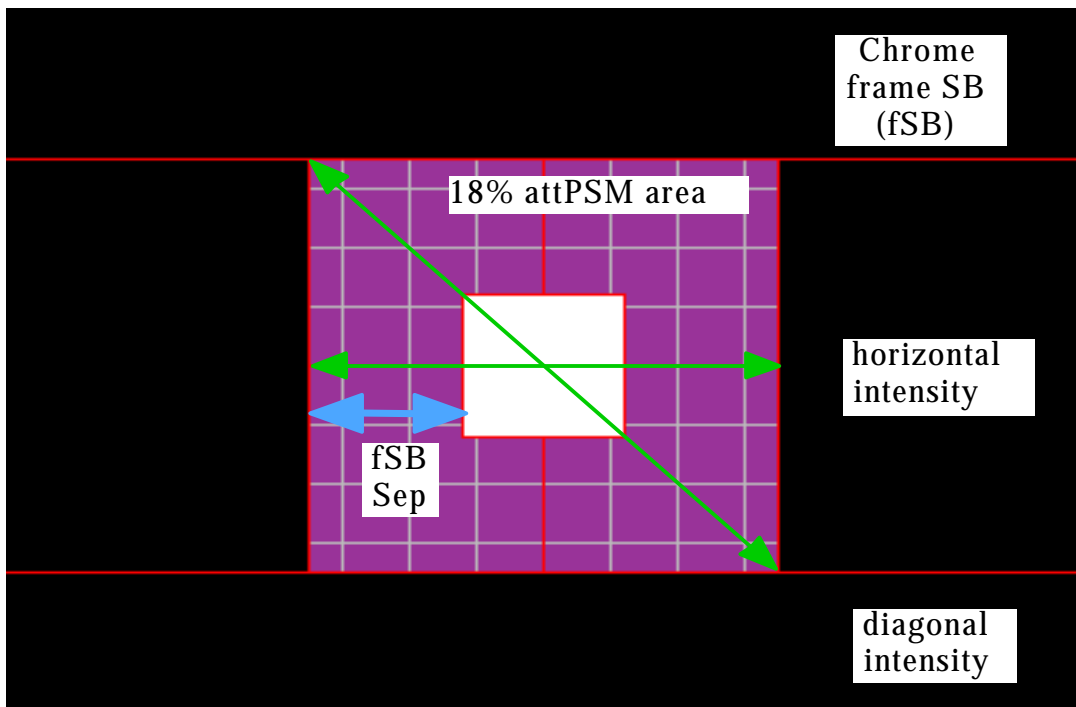
Figure 13. Design of the contact hole mask in which the Bessel contact hole electric field is made into three discrete tones. The while area is the quartz material, the gray area is the attenuating PSM material, and the black area is chrome.
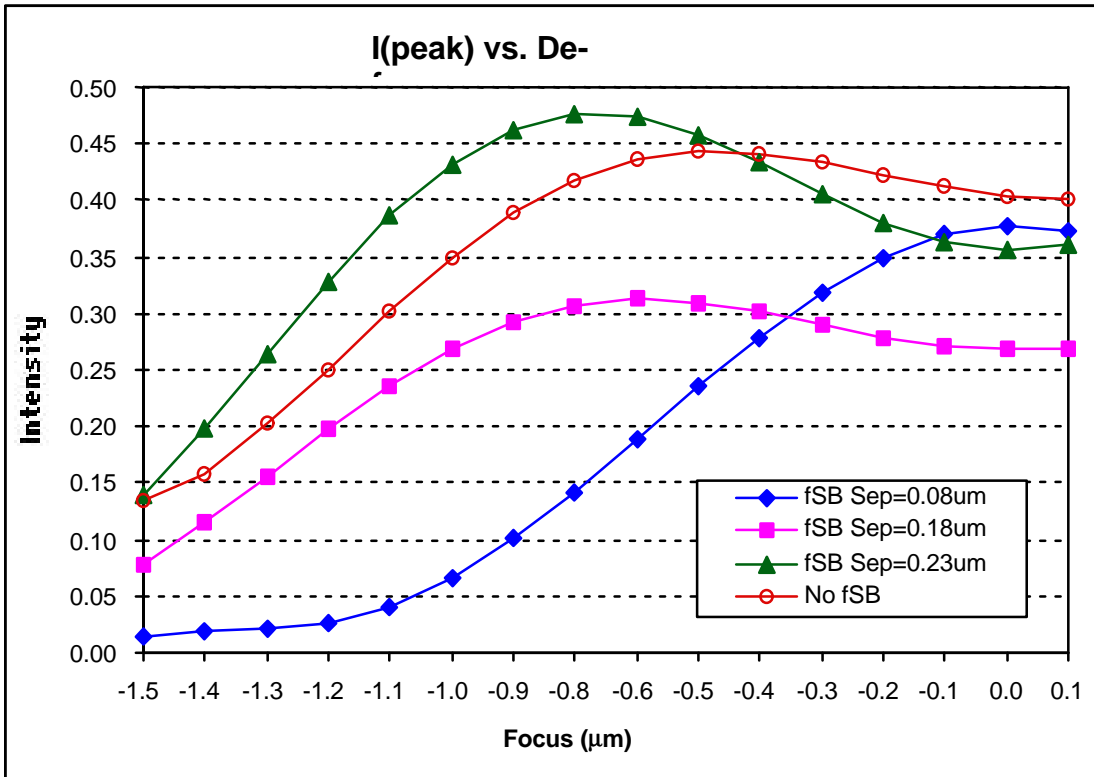
Figure 14. Effect of the frame scattering bar (SB) separation on the peak intensity through focus. The frame SB separation of 0.18μm is optimal since it has the least oscillation in peak intensity while maintaining the depth of focus.
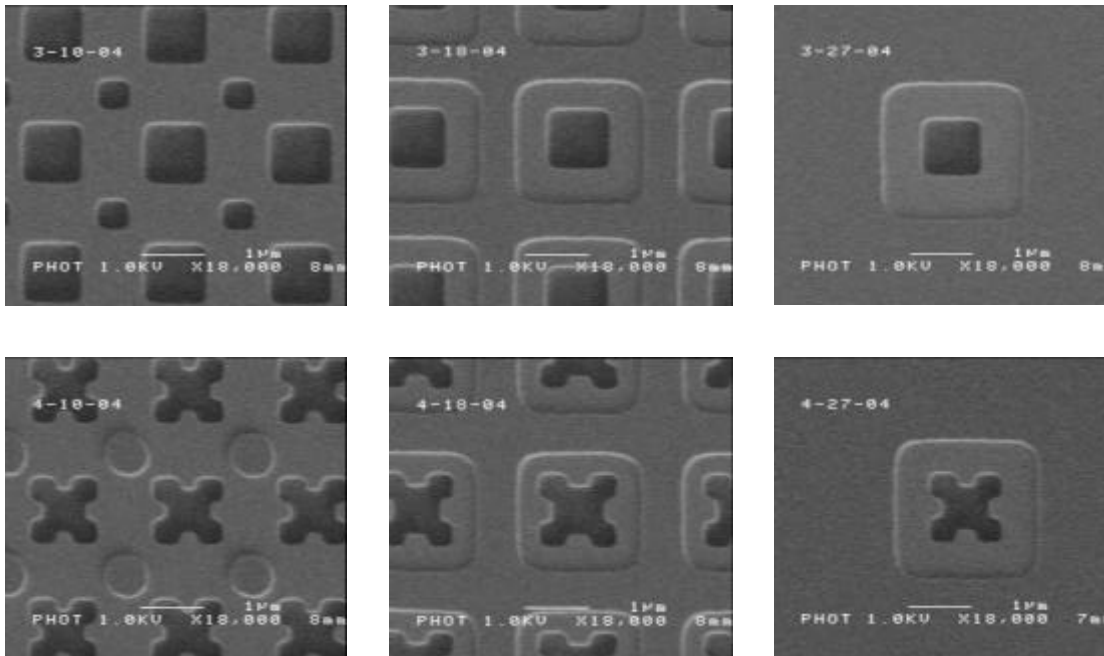
Figure 15. Reticle SEMs of typical Bessel contacts for various pitches and different OPC treatments.

Focus=+0.2μm Focus=+0.3μm Focus=+0.4μm

Focus=+0.1μm 0.51μm DOF @ 10% Exp. Lat. Focus=+0.5μm

Focus=0.0μm Focus=+0.6μm
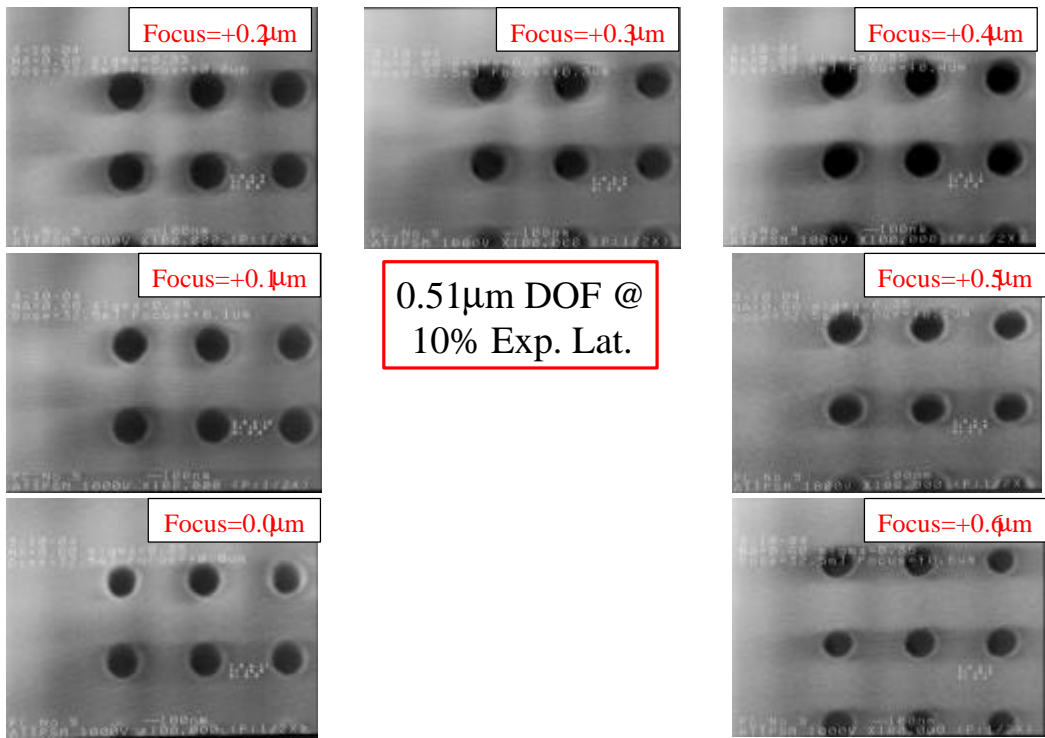
Figure 16. Effect of focus at best exposure on 160nm contacts with a pitch of 520nm. Note that the lack of side lobe printing and the same contact hole sizes for center, edge and corner holes.

Dose=30.0mJ/cm^2 Dose=32.5mJ/cm^2 Dose=35.0mJ/cm^2

Dose=27.5mJ/cm^2 0.51μm DOF @ 10% Exp. Lat. Dose=37.5mJ/cm^2

Dose=25.0mJ/cm^2 Dose=40.0mJ/cm^2
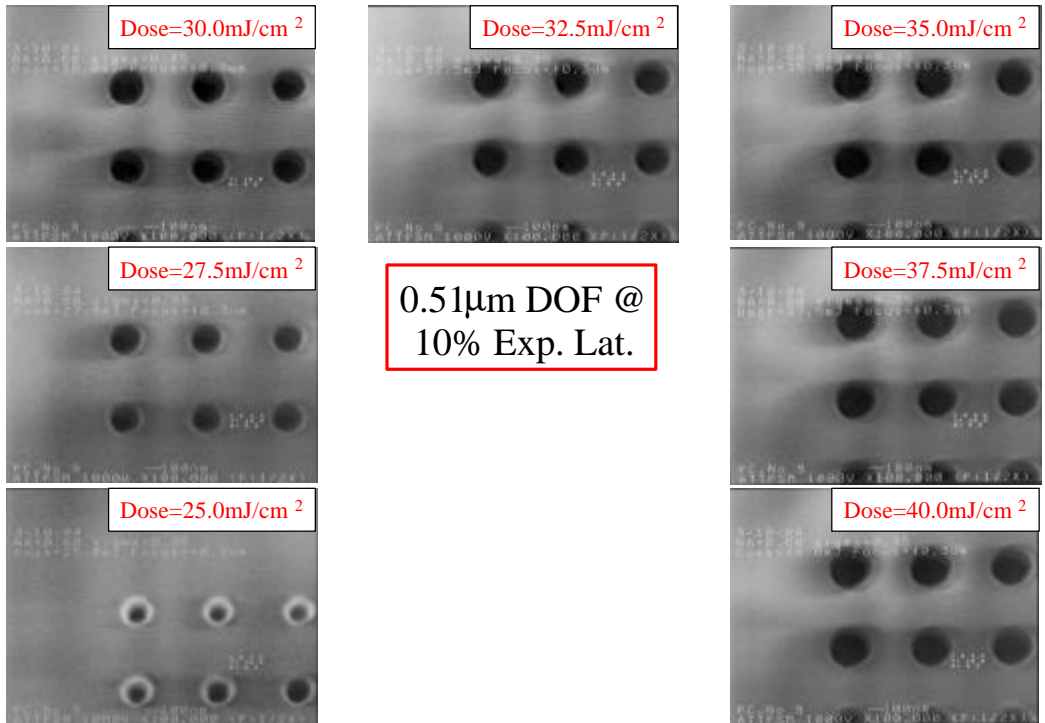
Figure 17. Effect of exposure at best focus on 160nm contacts with a pitch of 520nm.
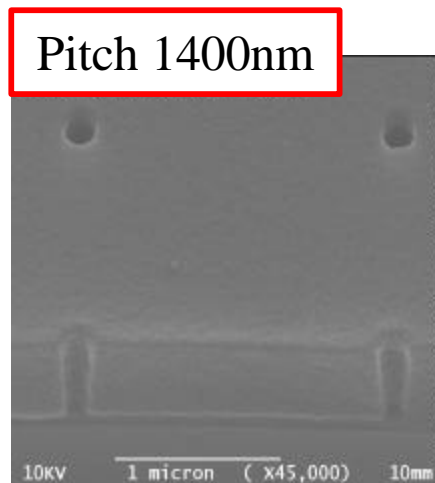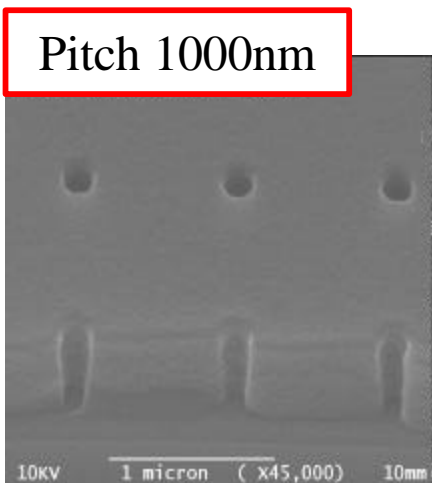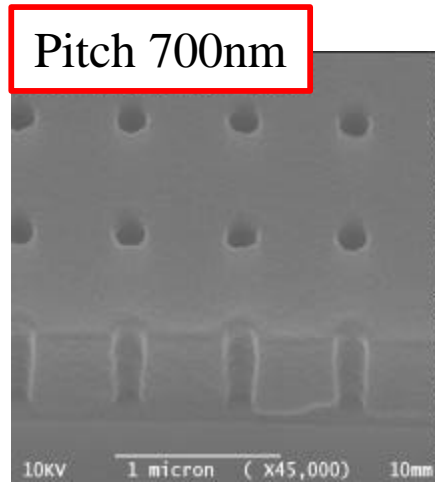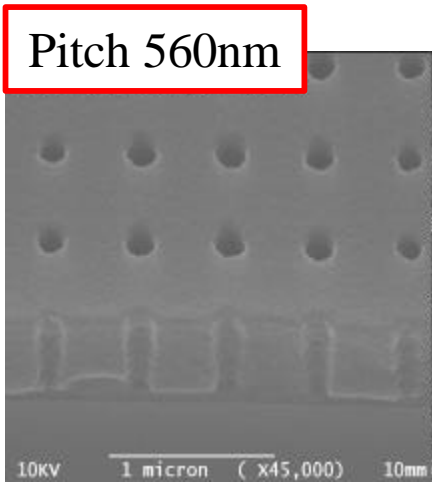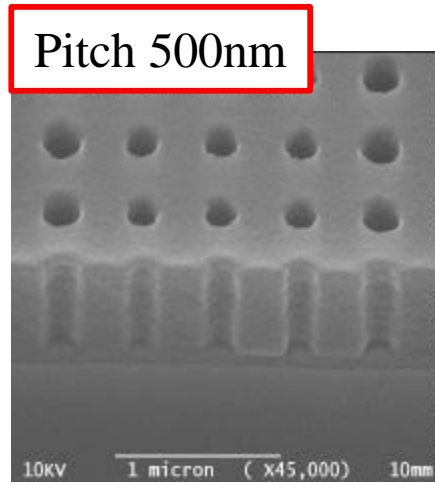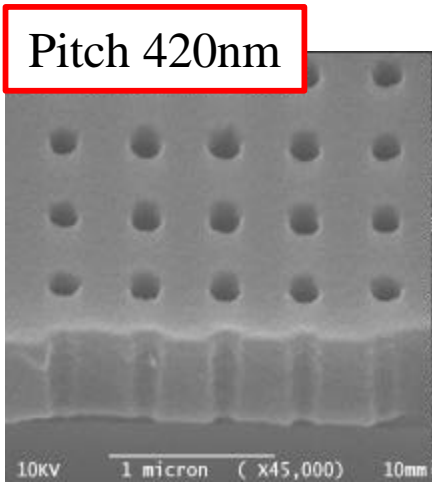
Figure 18. Cross section SEMs of 140nm contacts through pitch at best focus and best exposure for a NA of 0.60 and a σ of 0.35.

Figure 19. Exposure latitude versus depth of focus for 140nm contact with a 500nm pitch.

Figure 20. Exposure latitude versus depth of focus for 140nm contact with a 1400nm pitch.
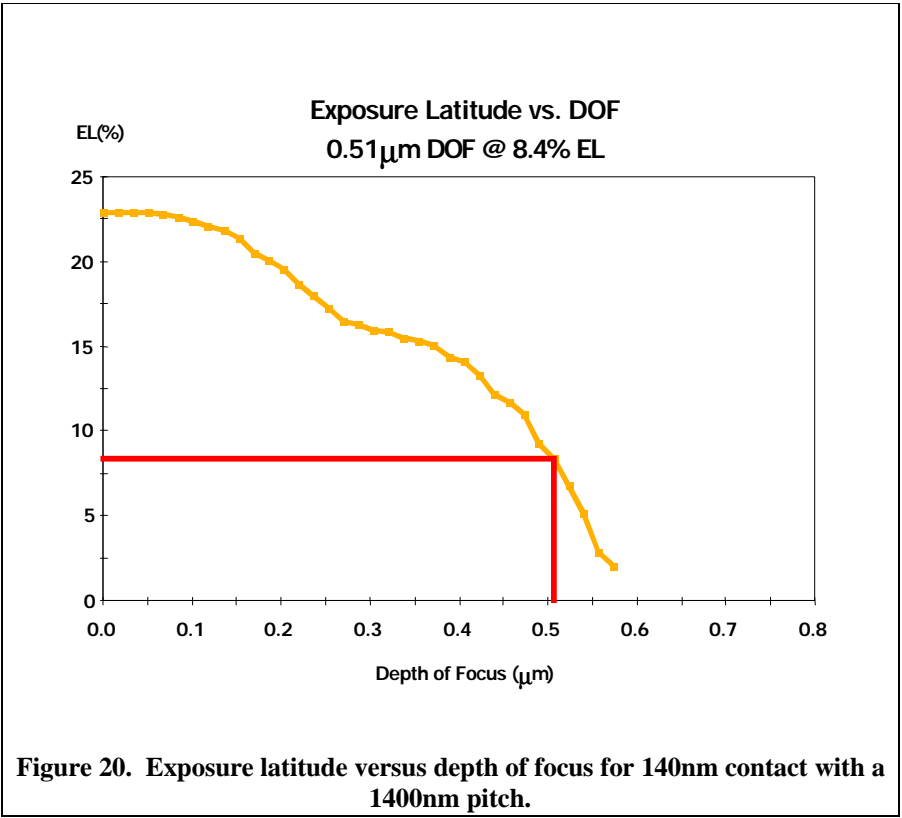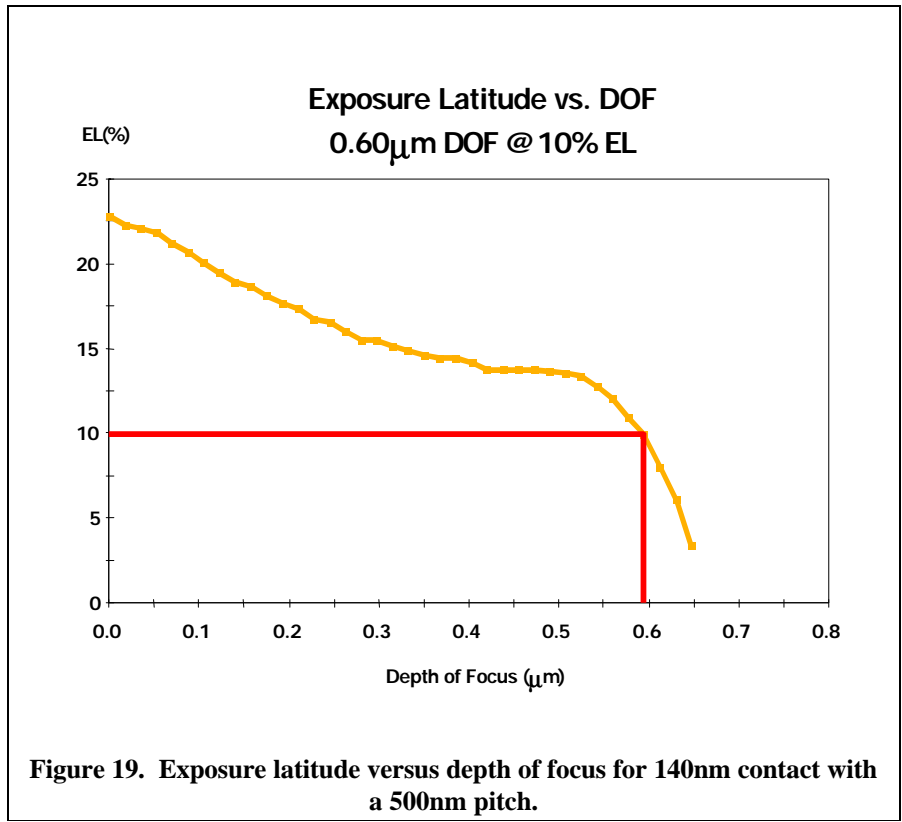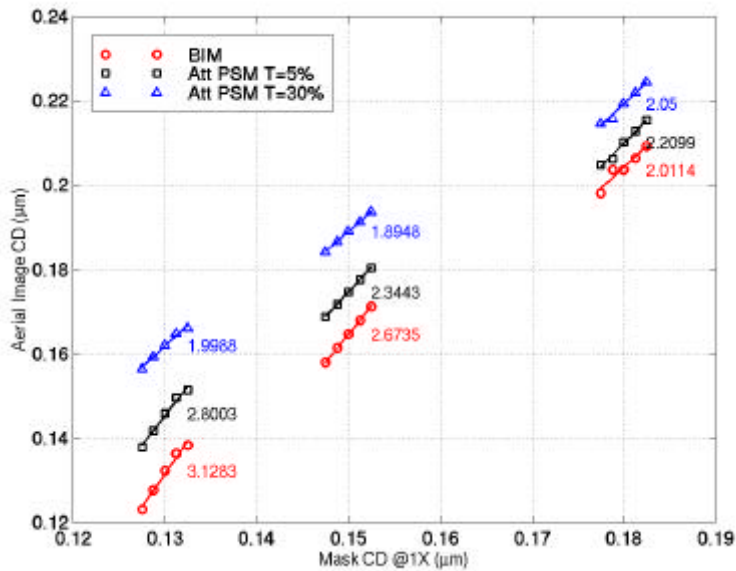
Figure 21. Simulations of MEF for attenuating PSM and BIM for an isolated line at 0.0μm with NA of 0.63 and σ of 0.75. Note that as the transmittance increases the MEF at the smaller mask CD dimensions decreases.
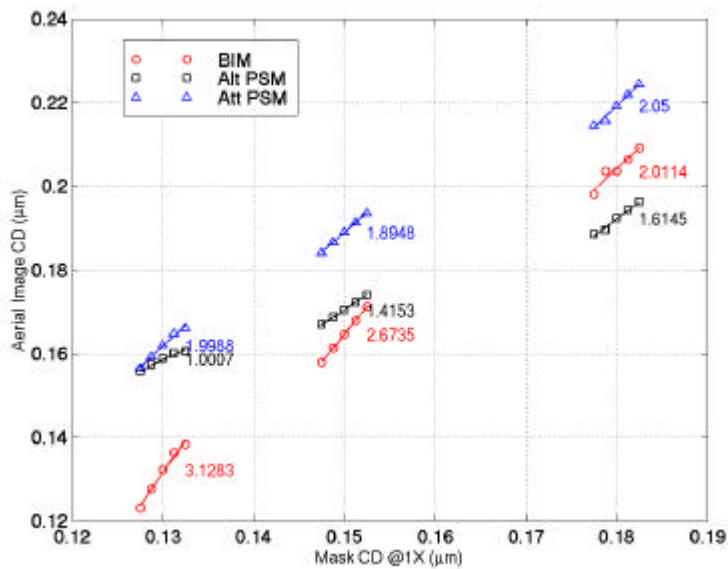
Figure 22. Simulations of MEF for BIM, 30% attenuating PSM and alternating PSM for an isolated line at 0.0μm with NA of 0.63. Note that the alternating PSM has lowest MEF at the smaller mask CD dimensions.
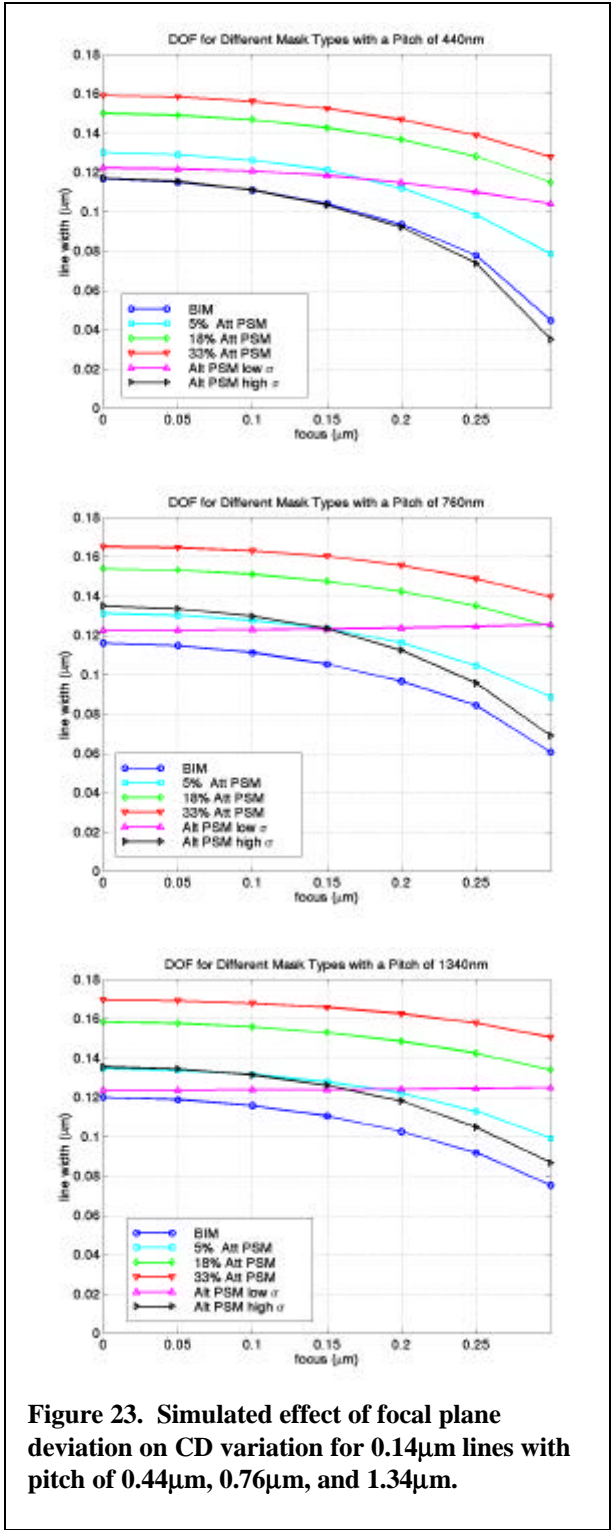
Figure 23. Simulated effect of focal plane deviation on CD variation for 0.14μm lines with pitch of 0.44μm, 0.76μm, and 1.34μm.
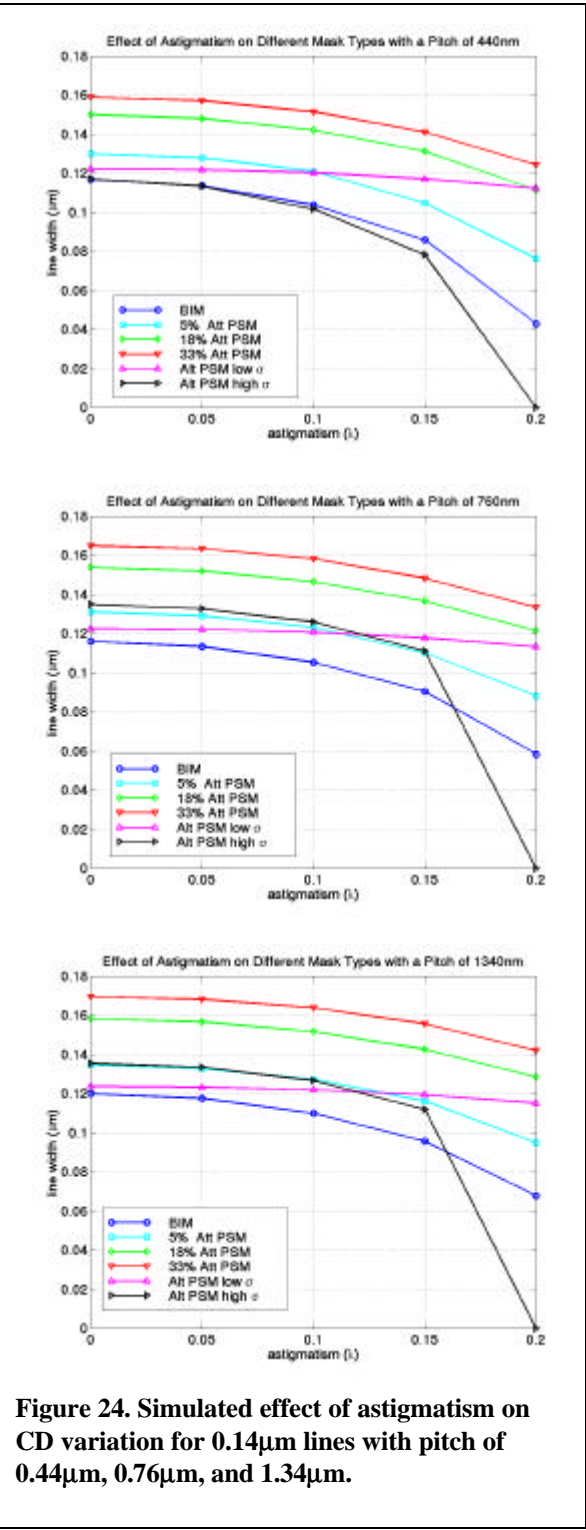
Figure 24. Simulated effect of astigmatism on CD variation for 0.14μm lines with pitch of 0.44μm, 0.76μm, and 1.34μm.
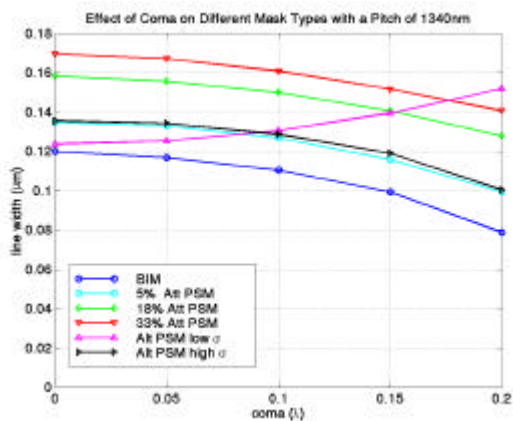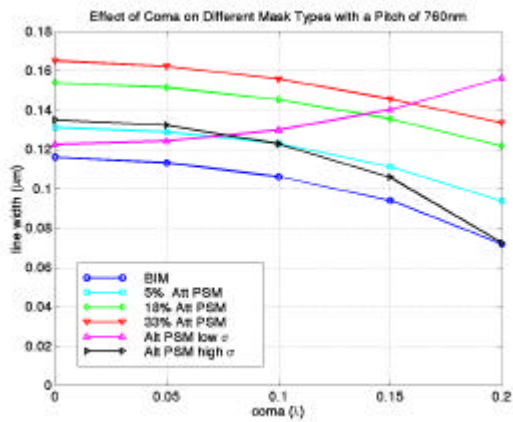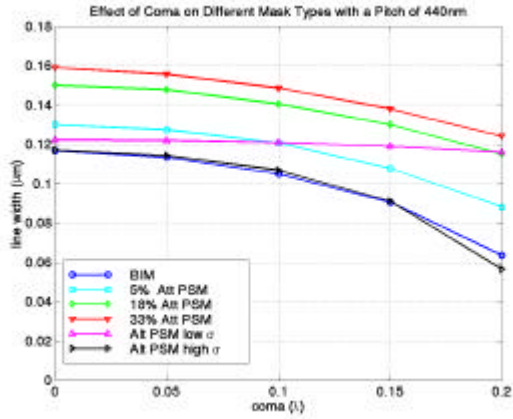
Figure 25. Simulated effect of x coma on CD variation for 0.14μm lines oriented along the y axis with pitch of 0.44μm, 0.76μm, and 1.34μm.
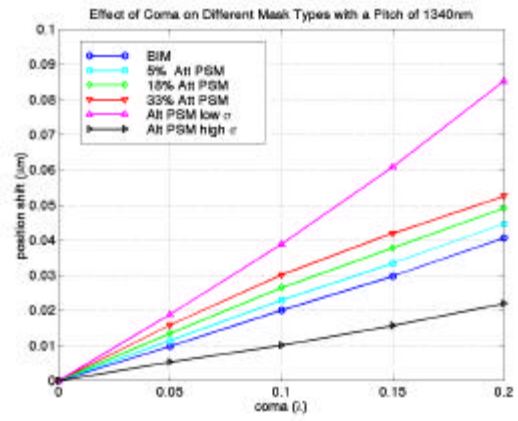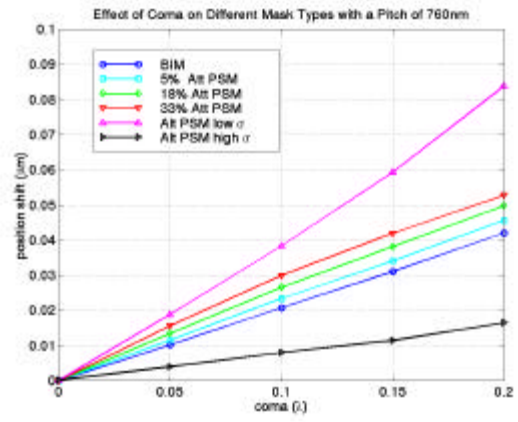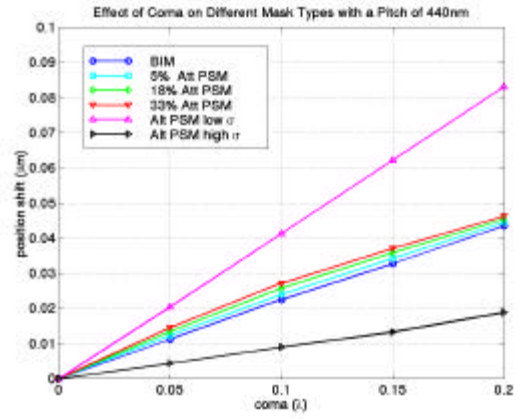
Figure 26. Simulated effect of x coma on CD placement error for 0.14μm lines oriented along the y axis with pitch of 0.44μm, 0.76μm, and 1.34μm.
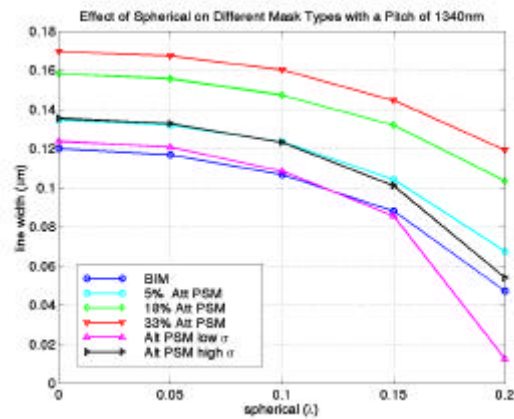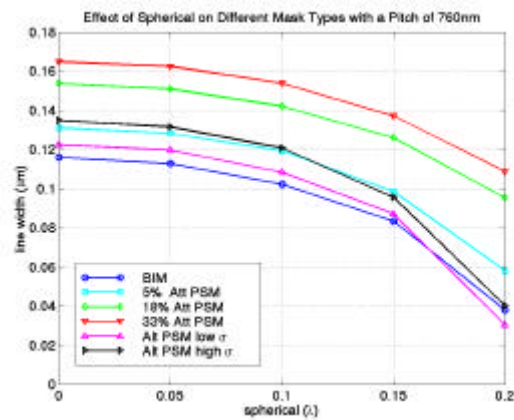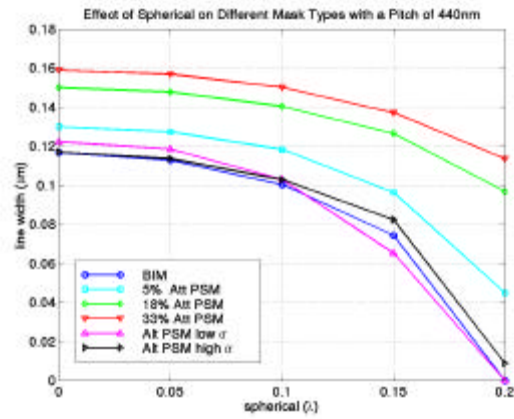
Figure 27. Simulated effect of spherical aberration on CD variation for 0.14μm lines oriented along the y axis with pitch of 0.44μm, 0.76μm, and 1.34μm.